JOINT EUROPEAN TORUS

JET–P(91)36

D. Pasini
and JET Team

Impurity Transport in JET

Impurity Transport in JET

D. Pasini
and JET Team*

JET-Joint Undertaking, Culham Science Centre, OX14 3DB, Abingdon, UK

** See Appendix 1*

Preprint of Paper to be submitted for publication in
Plasma Physics and Controlled Fusion

IMPURITY TRANSPORT IN JET

D.Pasini, R.Giannella, L.Lauro-Taroni, M.Mattioli[1],
B.Denne-Hinnov, N Hawkes[2], G.Magyar, H.Weisen[3]

JET Joint Undertaking, Abingdon, Oxon, UK

(1) Association EURATOM - CEA, Cadarache
(2) Association EURATOM - UKAEA, Culham
(3) Association EURATOM - Suisse, CRPP

ABSTRACT

Impurity transport has been studied in JET using the laser blow-off technique. Results are presented for Ohmic, L-mode and H-mode plasmas. In all cases impurity transport was found to be small inside r/a ~ 0.3 with values for D~.03-.3 m^2/s close to neoclassical predictions. Outside r/a~0.4, the transport was much faster than neoclassical with values for D~0.3-.6, 3-5 and 0.8-1.2 m^2/s in H-mode, L-mode and Ohmic plasmas, respectively. These values apply only between sawtooth crashes, during the sawtooth phase itself (~ 100 μs) the transport is greatly perturbed over the central region allowing the impurities to quickly leave or enter this region. In Ohmic plasma the impurity confinement time τ_{imp} was between 250 and 350 ms. This value was reduced to ~150-200 ms in L-mode plasma due to an increase of D in the anomalous transport region. During H-mode plasmas, on the other hand, very long impurity confinement times, of the order of several seconds, were observed. This was explained by a sharp increase of the ratio V/D in a thin region near the plasma edge and a general reduction of D in the outer-half of the plasma radius.

INTRODUCTION

The fusion performance of tokamak plasmas is negatively affected by the presence of impurities which lower the plasma temperature and dilute the reacting ions. It is recognised that the control of impurities is a pre-requisite for building a tokamak reactor. To achieve this end an adequate understanding of the impurity production mechanisms and their transport into the plasma is required.

Impurity transport is most easily studied using transient perturbative

methods. Injection of impurities by laser blow-off (Marmar et al., 1975) offers several advantages and it has been used in several experiments (Pasini et al., 1990 and references therein). In particular only a small quantity of impurity need to be injected thus avoiding any significant perturbations of the plasma parameters. Impurities can be injected at any selected time and the time history of the source is relatively well known with little or no recycling of the injected impurities. Furthermore the source duration is short compared to the characteristic transport time thus providing a more direct measurement of impurity transport.

The laser blow-off technique has been used in JET to study impurity transport in Ohmic, L-mode and H-mode discharges. The Ohmic and L-mode results have already been reported in a previous publications (Pasini et al.,1990). This paper contains additional information on the transport of impurities during the H-mode and presents an overview of the results obtained for the three regimes.

EXPERIMENTAL CONDITIONS AND DIAGNOSTICS

JET is a large D=shaped tokamak with major radius R_o=2.96 m, minor radius a=1.25 m, nominal toroidal field B_T=3.4 T, plasma current I_p up to 7 MA and plasma elongation up to 1.6. The experiments reported here were performed using limiter, single-null and double-null X-point discharges with the following plasma parameters: I_p= 3 MA, B_t= 3 T, $\langle n_e \rangle$=1-4 x 10^{19} m^{-3}, and T_e=4-9 keV.

A schematic of the laser blow-off impurity injection system is shown in Fig.1 (Magyar et al., 1989). The target chamber which contains glass slide targets coated with various materials is attached to the bottom of the vacuum vessel. When the laser is fired onto the target it vaporizes from its surface the thin layer of coated material (5 μm thick) producing a burst of impurities which can propagate towards the plasma. All the material within the 3-4 mm spot size is evaporated which corresponds to a few 10^{18} atoms: of these, only a fraction reaches the plasma center leading to impurity concentration of a few 10^{-4} n_e. The injected neutral particles have energies of the order of a few eV and reach the plasma boundary, 1.3 m away, in less than 1 ms. The atoms are ionized at the plasma edge and spread out rapidly along the field lines with toroidal velocity in the range of 10^4 m/s. At the same time, because of collisions or turbulence, the ions move slowly radially inwards with typical velocities of 1 to 10 m/s.

The progression of the impurities into the plasma was followed with good spatial and temporal resolution using two soft X-ray cameras (Edwards et al., 1986). The system uses 38 viewing lines in a vertically oriented fan and 62 in a horizontal fan providing a spatial resolution of 7 cm and a time resolution of 5 μs. It is absolutely calibrated within 5 % and allows tomographic reconstruction of the X-ray emission (Granetz and Smeulders, 1988). Many absorption filters are available to study the emission in different energy bands. A 250 μm Be filter was used in the present work which helped to discriminate the emission of the injected impurities from the background plasma emission but limited the measurement to the plasma region inside r/a ~ 0.9. Additional information, in particular on the plasma boundary, was obtained from measurements of spectroscopic line brightnesses time evolution using VUV and X-ray spectrometers. The profiles of the electron density and of the electron temperature needed for the simulations were obtained from interferometric measurements and from absolutely measured values of the electron cyclotron emission (ECE), respectively.

EXPERIMENTAL RESULTS

Fig.2 shows the time evolution of the Ni XXVI line brightness normalised to the electron density following the injection of Ni in Ohmic, L-mode and H-mode plasmas. The characteristic decay time, τ_{imp}, of the line intensity is a measure of the confinement time of the injected impurity. In Ohmic plasmas, τ_{imp} was between ~ 250 and 350 ms with a tendency to be larger at higher electron density. This value was independent of the type of impurity injected (τ_{imp} was the same using either Ti, Fe or Mo) and also did not depend on the value of Z_{eff}. With additional heating , in L-mode plasmas , τ_{imp} was reduced to values between ~ 150 and 200 ms. In H-mode plasmas, on the other hand, the value of τ_{imp} became of the order of several seconds with no difference between NBI heated and ICRF heated H-modes.

Ni injection into H-mode - Typical traces of a 3 MA, double null X-point, neutral beam heated H-mode shot are shown in Fig.3. The H_α trace shows the H-phase starting at 10.2 s, 200 ms after the beginning of beam heating, and lasting up to 12 s when the beam power is stepped down from 9 MW to 4 MW. The continuous rise of n_e is due to both beam fuelling and the improved particle confinement during the H-phase. Ni was injected near the middle of the H-mode at 10.985 s. The subsequent evolution of the Ni XXV and Ni XXVI

signals is given with an expanded time scale in Fig.3. The intensity step seen 100 ms after the initial rise on the Ni XXV signal is due to a small additional burst of Ni impurities. The constant intensity or very slow decay of the intensities indicate impurity confinement of the order of several seconds. Fig.4 shows the time evolution of the soft X-ray emissivity profiles (background emission subtracted) along a horizontal central chord. An increasingly hollow X-ray emission develops which indicates that from the plasma periphery to about r/a=0.4 the injected impurities travel very rapidly and from there on travel at a much slower pace.

The experimental data have been simulated using an impurity transport code where the radial flux density Γ_z was described as the sum of a diffusive and a convective term, $\Gamma_z = -D\ \nabla n_z + V\ n_z$. Both the diffusion coefficient D and the inward convection velocity V were taken to be a function of the radial coordinates and were specified, independently, to best reproduce the experimental data, namely, the X-ray emissivity profiles and the spectroscopic line brightnesses time evolution. The shape of the source function was taken so as to reproduce the time evolution of peripheral Ni lines (FWHM ~ 20 ms). In order to reproduce the X-ray emission profiles it was necessary to assume two distinct transport regions: in the central region (whose radial size had to be such as to match the hollowness of the experimental data) the diffusion coefficient needed is much lower than in the outer region. The calculated soft X-ray emissivity profiles are shown in Fig.4 (dashed lines) for comparison with the measured profiles, together with the corresponding Ni density profiles also calculated with the same code (lower part of Fig.4).The transport parameter curves which have been used to describe the transport of Ni during the quiescent phase of the sawteeth are shown in Fig.5 along with the corresponding curves used to describe the transport behaviour of OH and ICRF heated L-mode plasmas (Pasini at al.,1990). The dramatic effect of a sawtooth crash on impurity transport which can be seen in Fig.4 will be discussed in a latter section.

During the H-mode the ratio V/D needs to be increased by a factor 50 or more, compared to L-mode values, in a thin region near the plasma edge (Giannella et al.,1989,1990; Hawkes et al.,1989). The appearance of this convective barrier may be related to the localised edge perpendicular electric field which has been shown to appear at the L-H transition (Groebner et al., 1990). At present we are not able to determine the transport parameters beyond r/a=0.9: the simulations show that we cannot

discriminate between a constant D up to the plasma edge coupled with a sharply increasing V to a high value ($V_a \cdot a / D_a > 100$) and a possible abrupt drop of D near the edge to a neoclassical value ($D_a < 0.08$ m^2/s) with a more modest increase of V in the same region. In this second case the ratio $V_a \cdot a/D_a$ is higher than in the first case. In the simulation presented here D, which was determined from the evolution of soft X-ray profiles in the plasma interior (D= 0.4 m^2/s), was assumed to be constant up to the plasma edge. With this assumption a value of 50 m/s was required for V at the edge compared to approximately 2 m/s and 6 m/s in Ohmic and L-mode plasmas (Pasini et al.,1990). The thickness Δr of the zone where a higher inward velocity is needed was determined from the behaviour of the Ni XXV line and of lines from lower ionization stages which are very sensitive to this parameter.

H-modes into which impurities were injected sometimes evolved into a new regime where the particle and impurity confinement were reduced by approximately a factor 3 while the energy confinement was degraded by a much lower factor of ~20 % (Bures et al.,1991). The simulation of these data showed that the impurity diffusion coefficient reverted to near L-mode values in the plasma interior but that the transport barrier at the edge was not strongly affected. Similarly L-mode plasmas near the H-mode threshold showed the build up of a convective barrier at the edge while the values of D were still typical of L-mode in the plasma interior. The significance of these observations is not yet analysed.

Comparison between OH, L-mode and H-mode transport - The results of the experiments for Ohmic, L-mode and H-mode show that the impurity diffusion coefficient is always much lower in the central region of the plasma than in the outer region, during the quiescent phase of the sawteeth, and that the transition between these two regions is rather abrupt. A similar strong reduction of the diffusion coefficient in the central region was also reported by Compant La Fontaine et al. (1985). The values of D over the central region where the confinement is good (low D) are of similar magnitude in the three cases. However, this region is more extended in the H-mode case and the transition region is more gradual. For the plasma pulses analysed here these values are 0.03, 0.15 and 0.1 m^2/s in the OH, L-mode and H-mode case, respectively, which compare well with the corresponding neoclassical values which are, taking into account collisions with the

deuterium ions and background impurities, 0.04, .07, and 0.1 m^2/s, respectively. In the outer region , the values of D are 1, 3 and 0.4 m^2/s. They are much larger than the corresponding neoclassical values which are 0.06, 0.06 and 0.08 m^2/s.

Even in discharges with q(0)>1 a similar sharp reduction of the diffusion coefficient around r/a~0.3 was required to explain the transport of intrinsic and injected impurities. The accumulation of impurities on axis which is often observed in the early phase of the discharge before the onset of sawteeth, as shown in the example of Fig.6 (Gill et al.,1991), provides further evidence of the low value of the impurity diffusion coefficient in the central region of the plasma. Also central pellet injection often result in long lasting very peaked density profile which can only be explained by a reduced diffusion coefficient in the inner part of the discharge (Giannella et al.,1991). Only sawteeth seems to counteract this inner zone of low diffusivity found in all type of discharges.

Sawteeth effects - During a sawtooth crash (~100 μs) the soft X-ray data show that impurity transport is greatly enhanced over the central region of the plasma up to a mixing radius roughly 30 % larger than the sawteeth inversion radius. In the case of laser impurity injection, when the impurity distribution is hollow during the inflow phase, a sawtooth crash allows for a rapid inward movement of the impurities which can quickly fill the central plasma region (Seguin et al.,1983). This effect can be seen in Fig.4 where the X-ray profiles just before and immediatly after a sawtooth crash are shown together with the corresponding impurity density profiles on the lower part of the figure. In the simulation the sawtooth discontinuity was simulated by taking ad-hoc enhanced transport parameters which reproduce the X-ray emissivity profile variation and the intensity jump visible only on the Ni XXVI line (Fig.2). Once the impurities have peaked in the plasma center the reversed effect can be seen during the outflow phase, i.e. the impurities are expelled from the central region at each sawtooth crash, as shown in Pasini et al.(1990). Sawteeth therefore allow for much more rapid movement of impurities between the central region and the outside and effectively short-circuit these two distinct transport regions. When the sawtooth period is much shorter than the impurity confinement time the transport of impurities is effectively controlled by the value of D in the anomalous transport region.

CONCLUSION

The laser blow-off technique has been used in JET to study impurity transport. The radial dependencies of the impurity transport parameters D and V were obtained by simulating the time evolution of the soft X-ray profile and line brightnesses time evolution following impurity injection. Both Ohmic, L-mode and H-mode plasmas have been investigated. In all cases it was found that D was small inside r/a~0.3 with values close to neoclassical predictions while in the more outer region the values of D were anomalous. During sawtooth crashes the transport was greatly enhanced in the central region up to the mixing radius and this effectively short-circuited the two transport regions allowing for a quick movement of impurities accross the full plasma diameter. The values of D in the anomalous transport region were larger during L-mode than during Ohmic plasmas resulting in lower values for τ_{imp}. During H-mode plasmas D was smaller in the anomalous transport region compared to L-mode plasmas and the ratio $V \cdot a/D$ was increased by a factor 50 or more in a thin region (~0.1 m) at the plasma edge. This explained the dramatic increase, by more than a factor of ten, of the impurity confinement time during the H-mode.

Acknowledgements: Contributions and valuable discussions with K Lawson and D Boucher are gratefully acknowledged.

References

Bures M., Campbell D., Gottardi N. et al.(1991) to be published.

Compant La Fontaine A., Dubois M.A., Pecquet A.L. et al.(1985), Plasma Phys.Controll.Fusion **27**,229.

Edwards A.W., Fahrbach H.U., Gill R.D. et al.(1986), Rev.Sci.Instrum.**57**, 2142.

Giannella R., Behringer K., Denne B. et al. (1989), Proc. 16th Conf. on Controlled Fusion and Plasma Physics, Venice, Vol I-209.

Giannella R., Lauro-Taroni L., Barnsley R. et al.(1990), Proc. 17th European Conf. on Controlled Fusion and Plasma Physics, Amsterdam, Vol.I-247.

Giannellla R., Hawkes N.C., Lauro-Taroni L. et al.(1991), Proc. 18th Conf. on Controlled Fusion and Plasma Physics, Berlin, Vol.I-197.

Gill R.D., Edwards A.W., Pasini D. et al.(1991) Proc. 18th Conf. on

Controlled Fusion and Plasma Physics, Berlin, Vol II-49.

Granetz R.S.and Smeulders P.(1988), Nucl.Fusion **28**,457.

Groebner R.J., Burrel K.H., Seraydarian R.P.(1990) Phys.Rev.Lett. **64**, 3015.

Hawkes N., Wang Z., Barnsley R. et al.(1989), Proc.16 th European Conf. on Controlled Fusion and Plasma Physics, Venice, Vol. I-79.

Magyar G., Barnes M., Edwards A.W. et al.(1988)., JET Rep. JET-R(88)15.

Marmar E.S., Cecchi J.L. and Cohen S.A.(1975) Rev.Sci.Instrum. **46**,1149.

Pasini D., Mattioli M., Edwards A.W. et al.(1990), Nuclear Fusion **30**,2049.

Seguin F. H., Petrasso R., Marmar E.S.(1983)., Phys.Rev.Lett. **51**,455.

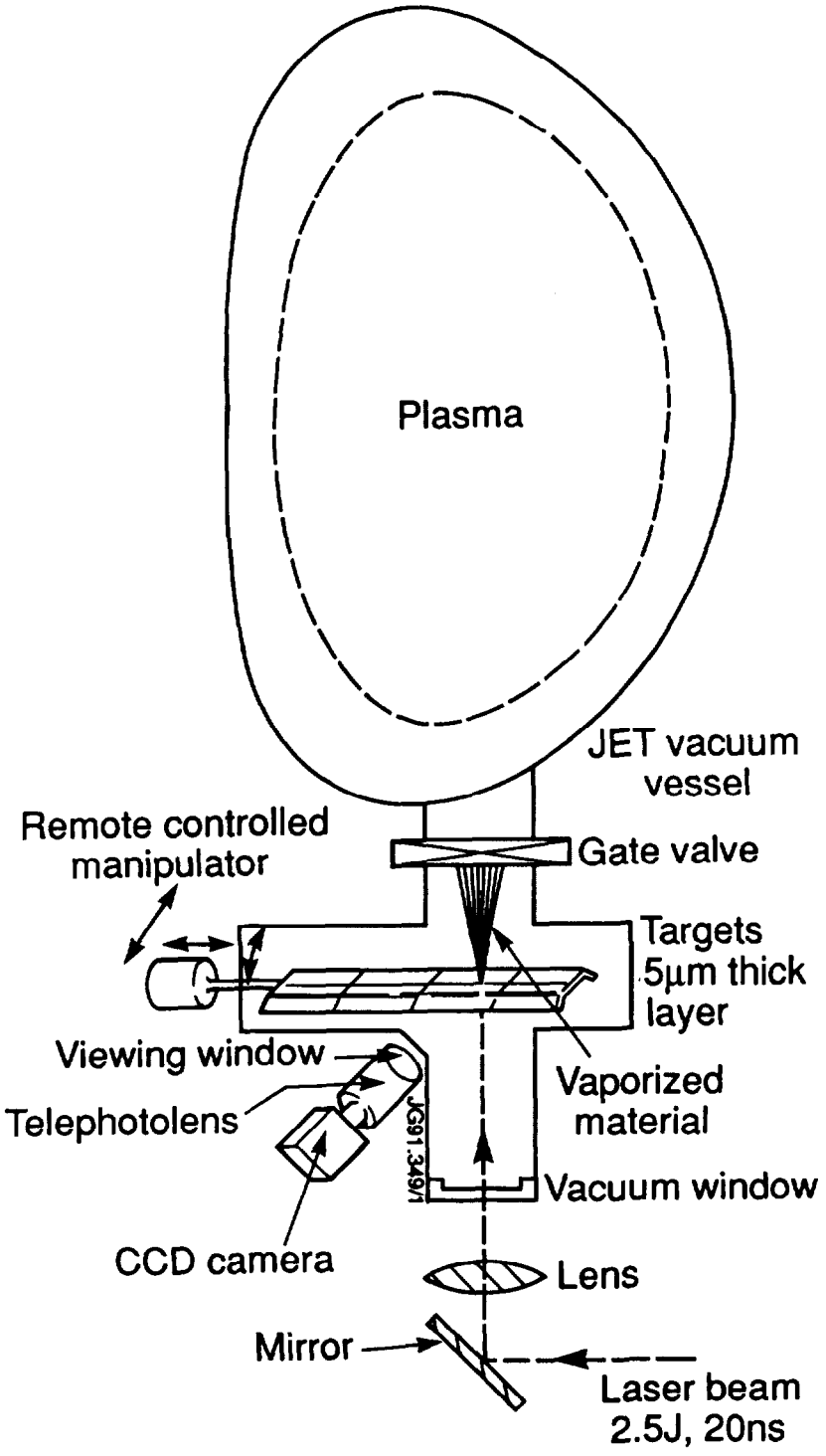

Fig.1 Schematic of the laser blow-off impurity injection system

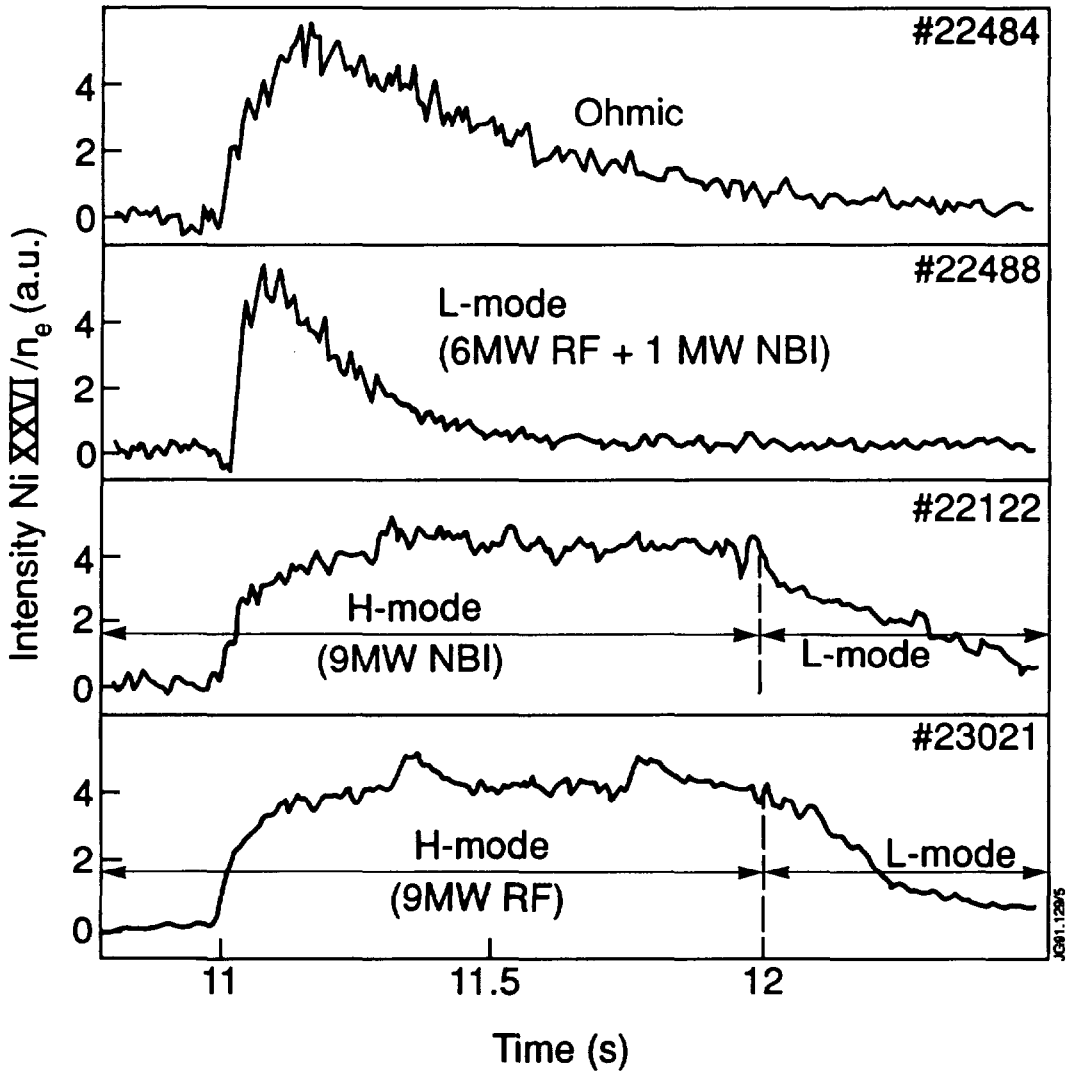

Fig.2 Evolution of the Ni XXVI brightnesses divided by the electron density following Ni injection into OH, L-mode and H-mode plasmas.

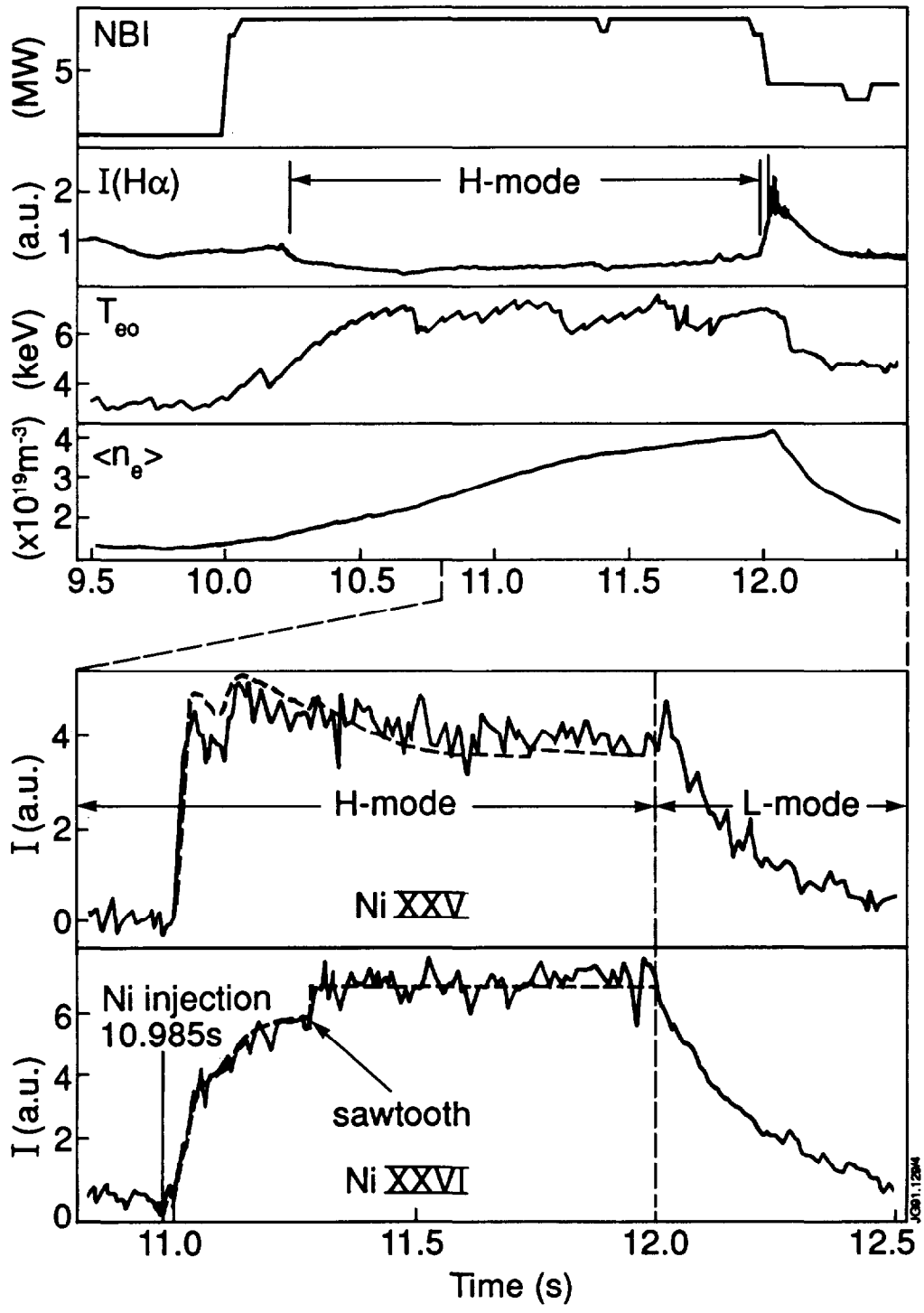

Fig.3 Plasma parameters for plasma shot #22122. The Ni XXV and Ni XXVI are shown with an expanded time scale. The dashed lines show the result of a simulation.

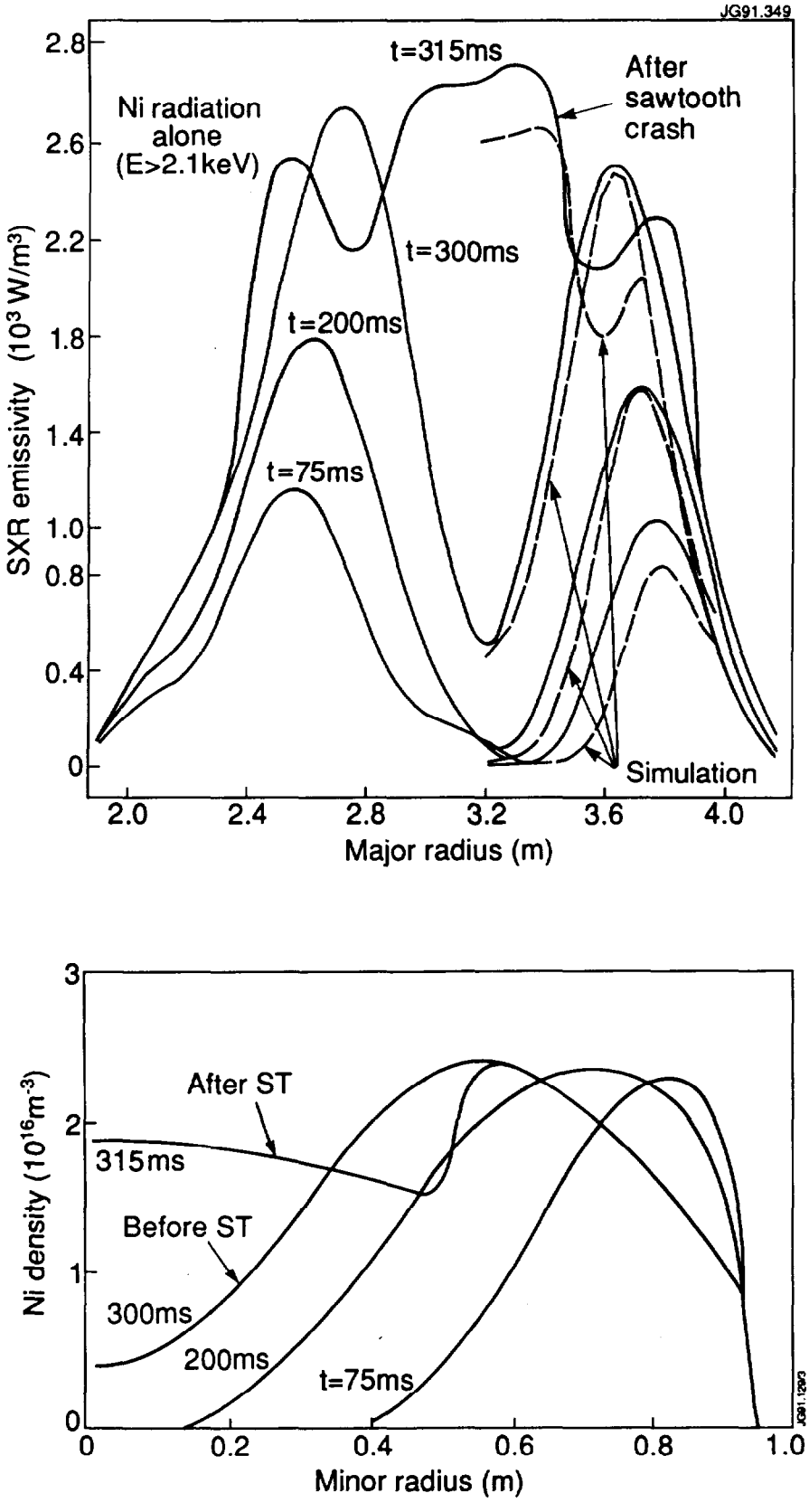

Fig.4 (top):Time evolution of the tomographically reconstructed X-ray emissivity distribution (background emission subtracted) along a horizontal central chord after Ni injection (shot #22122). The dashed lines show the result of a simulation. (bottom) : Calculated Ni density profiles at the corresponding times.

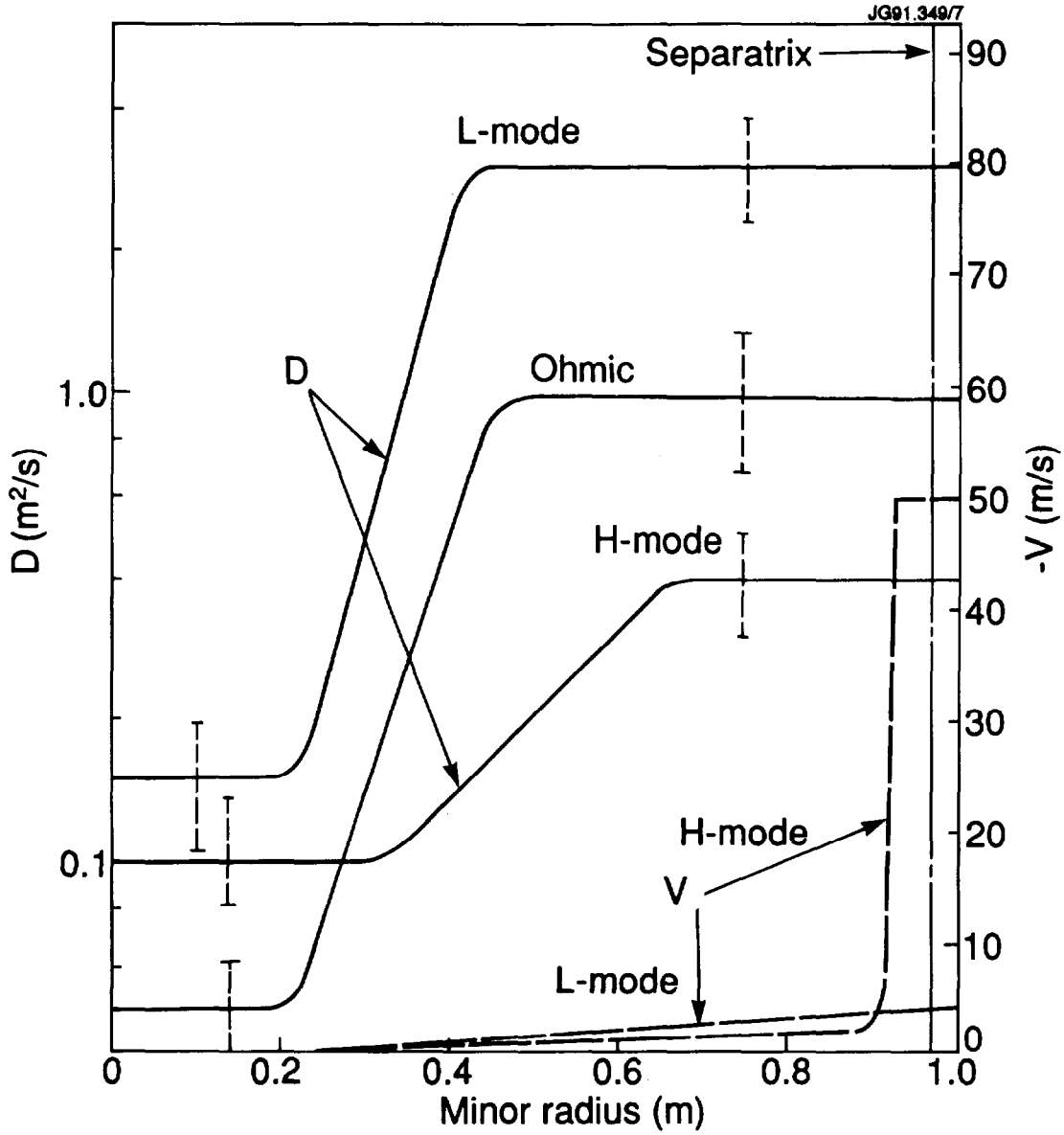

Fig.5 Radial profile of D (logarithmic scale on the left) and of V (linear scale on the right) determined for OH (#17661), L-mode (#18112) and H-mode plamas (#22122).

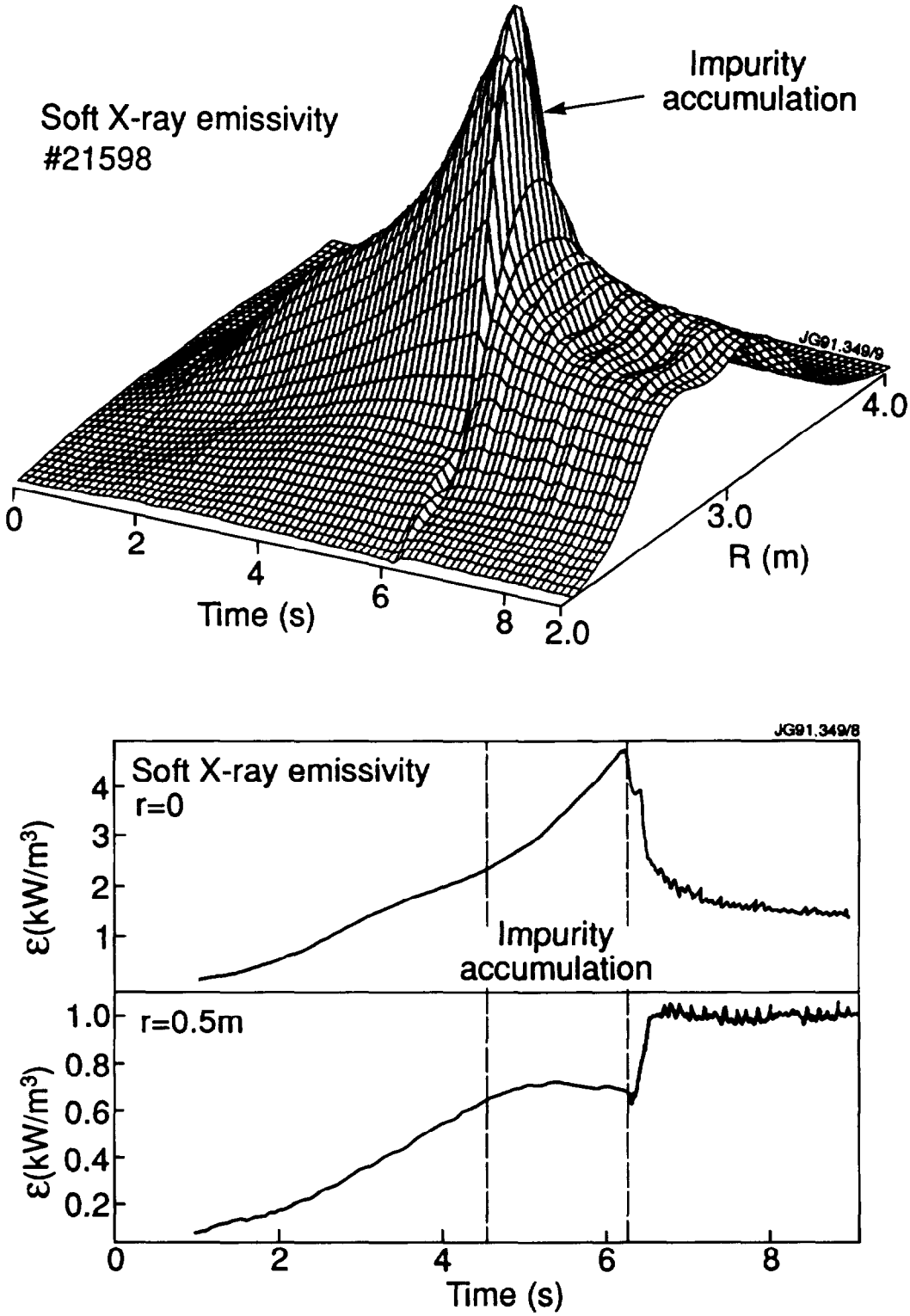

Fig.6 (top) Evolution of the soft X-ray emissivity profile showing the acuumulation of Cl impurities in the centre of the discharge before the onset of sawteeth. (bottom) Evolution of the local X-ray emissivity at r=0 and r=0.5 m showing better the accumulation phase and the expulsion of impurities from the central region when sawteeth begin (#21598)

Appendix I

THE JET TEAM

JET Joint Undertaking, Abingdon, Oxon, OX14 3EA, U.K.

J.M. Adams[1], H. Altmann, A. Andersen[14], P. Andrew[18], M. Angelone[29], S.A. Arshad, W. Bailey, P. Ballantyne, B. Balet, P. Barabaschi, R. Barnsley[2], M. Baronian, D.V. Bartlett, A.C. Bell, I. Benfatto[5], G. Benali, H. Bergsaker[11], P. Bertoldi, E. Bertolini, V. Bhatnagar, A.J. Bickley, H. Bindslev[14], T. Bonicelli, S.J. Booth, G. Bosia, M. Botman, D. Boucher, P. Boucquey, P. Breger, H. Brelen, H. Brinkschulte, T. Brown, M. Brusati, T. Budd, M. Bures, T. Businaro, P. Butcher, H. Buttgereit, C. Caldwell-Nichols, D.J. Campbell, P. Card, G. Celentano, C.D. Challis, A.V.Chankin[23], D. Chiron, J. Christiansen, C. Christodoulopoulos, P. Chuilon, R. Claesen, S. Clement, E. Clipsham, J.P. Coad, M. Comiskey[4], S. Conroy, M. Cooke, S. Cooper, J.G. Cordey, W. Core, G. Corrigan, S. Corti, A.E. Costley, G. Cottrell, M. Cox[7], P. Cripwell, H. de Blank[15], H. de Esch, L. de Kock, E. Deksnis, G.B. Denne-Hinnov, G. Deschamps, K.J. Dietz, S.L. Dmitrenko, J. Dobbing, N. Dolgetta, S.E. Dorling, P.G. Doyle, D.F. Düchs, H. Duquenoy, A. Edwards, J. Ehrenberg, A. Ekedahl, T. Elevant[11], S.K. Erents[7], L.G. Eriksson, H. Fajemirokun[12], H. Falter, D. Flory, J. Freiling[15], C. Froger, P. Froissard, K. Fullard, M. Gadeberg, A. Galetsas, D. Gambier, M. Garribba, P. Gaze, R. Giannella, A. Gibson, R.D. Gill, A. Girard, A. Gondhalekar, C. Gormezano, N.A. Gottardi, C. Gowers, B.J. Green, R. Haange, G Haas, A. Haigh, G. Hammett[6], C.J. Hancock, P.J. Harbour, N.C. Hawkes[7], P. Haynes[7], J.L. Hemmerich, T. Hender[7], F.B. Herzog, R.F. Herzog, J. Hoekzema, J. How, M. Huart, L Hughes, T.P. Hughes[4], M. Hugon, M. Huguet, A. Hwang[7], B. Ingram, M. Irving, J. Jacquinot, H. Jaeckel, J.F. Jaeger, G. Janeschitz[13], S. Jankowicz[22], O.N. Jarvis, F. Jensen, E.M. Jones, L.P.D.F. Jones, T.T.C. Jones, J-F. Junger, E. Junique, A. Kaye, B.E. Keen, M. Keilhacker, G.J. Kelly, W. Kerner, R. Konig, A. Konstantellos, M. Kovanen[20], G. Kramer[15], P. Kupschus, R. Lässer, J.R. Last, B. Laundy, L. Lauro-Taroni, K. Lawson[7], M. Lennholm, A. Loarte, R. Lobel, P. Lomas, M. Loughlin, C. Lowry, B. Macklin, G. Maddison[7], G. Magyar, W. Mandl[13], V. Marchese, F. Marcus, J. Mart, E. Martin, R. Martin-Solis[8], P. Massmann, G. McCracken[7], P. Meriguet, P. Miele, S.F. Mills, P. Millward, R. Mohanti[17], P.L. Mondino, A. Montvai[3], S. Moriyama[28], P. Morgan, H. Morsi, G. Murphy, M. Mynarends, R. Myrnäs[16], C. Nardone, F. Nave[21], G. Newbert, M. Newman, P. Nielsen, P. Noll, W. Obert, D. O'Brien, J. O'Rourke, R. Ostrom, M. Ottaviani, M. Pain, F. Paoletti, S. Papastergiou, D. Pasini, A. Peacock, N. Peacock[7], D. Pearson[12], R. Pepe de Silva, G. Perinic, C. Perry, M. Pick, R. Pitts[7], J. Plancoulaine, J-P. Poffé, F. Porcelli, L. Porte[19], R. Prentice, S. Puppin, S. Putvinsko[23], G. Radford[9], T. Raimondi, M.C. Ramos de Andrade, P-H. Rebut, R. Reichle, E. Righi, F. Rimini, D. Robinson[7], A. Rolfe, R.T. Ross, L. Rossi, R. Russ, P. Rutter, H.C. Sack, G. Sadler, G. Saibene, J.L. Salanave, G. Sanazzaro, A. Santagiustina, R. Sartori, C. Sborchia, P. Schild, M. Schmid, G. Schmidt[6], B. Schunke, S.M. Scott, A. Sibley, R. Simonini, A.C.C. Sips, P. Smeulders, R. Stankiewicz[27], M. Stamp, P. Stangeby[18], D.F. Start, C.A. Steed, D. Stork, P.E. Stott, T.E. Stringer, P. Stubberfield, D. Summers, H. Summers[19], L. Svensson, J.A. Tagle[21], A. Tanga, A. Taroni, A. Tesini, P.R. Thomas, E. Thompson, K. Thomsen, J.M. Todd, P. Trevalion, B. Tubbing, F. Tibone, E. Usselmann, H. van der Beken, G. Vlases, M. von Hellermann, T. Wade, C. Walker, R. Walton[6], D. Ward, M.L. Watkins, M.J. Watson, S. Weber[10], J. Wesson, T.J. Wijnands, J. Wilks, D. Wilson, T. Winkel, R. Wolf, B. Wolle[24], D. Wong, C. Woodward, Y. Wu[25], M. Wykes, I.D. Young, L. Zannelli, Y. Zhu[26], W. Zwingmann.

PERMANENT ADDRESSES

1. UKAEA, Harwell, Didcot, Oxon, UK.
2. University of Leicester, Leicester, UK.
3. Central Research Institute for Physics, Academy of Sciences, Budapest, Hungary.
4. University of Essex, Colchester, UK.
5. ENEA-CNR, Padova, Italy.
6. Princeton Plasma Physics Laboratory, New Jersey, USA.
7. UKAEA Culham Laboratory, Abingdon, Oxon, UK.
8. Universidad Complutense de Madrid, Spain.
9. Institute of Mathematics, University of Oxford, UK.
10. Freien Universität, Berlin, F.R.G.
11. Swedish Energy Research Commission, S-10072 Stockholm, Sweden.
12. Imperial College of Science and Technology, University of London, UK.
13. Max Planck Institut für Plasmaphysik, Garching bei München, FRG.
14. Risø National Laboratory, Denmark.
15. FOM Instituut voor Plasmafysica, 3430 Be Nieuwegein, The Netherlands.
16. University of Lund, Sweden.
17. North Carolina State University, Raleigh, NC, USA
18. Institute for Aerospace Studies, University of Toronto, Downsview, Ontario, Canada.
19. University of Strathclyde, 107 Rottenrow, Glasgow, UK.
20. Nuclear Engineering Laboratory, Lapeenranta University, Finland.
21. CIEMAT, Madrid, Spain.
22. Institute for Nuclear Studies, Otwock-Swierk, Poland.
23. Kurchatov Institute of Atomic Energy, Moscow, USSR
24. University of Heidelberg, Heidelberg, FRG.
25. Institute for Mechanics, Academia Sinica, Beijing, P.R. China.
26. Southwestern University of Physics, Leshan, P.R. China.
27. RCC Cyfronet, Otwock Swierk, Poland.
28. JAERI, Naka Fusion Research Establishment, Ibaraki, Japan.
29. ENEA, Frascati, Italy.

At 1st June 1991